Available online at www.sciencedirect.com
ScienceDirect
International Journal of Mass Spectrometry 269 (2008) 210–220
International Journal of Mass Spectrometry
www.elsevier.com/locate/ijms

Near-threshold absolute photoionization cross-sections of some reaction intermediates in combustion

Juan Wang [a], Bin Yang [a], Terrill A. Cool [a,*], Nils Hansen [b], Tina Kasper [b]

[a] *School of Applied and Engineering Physics, Cornell University, 228 Clark Hall, Ithaca, NY 14853, USA*
[b] *Combustion Research Facility, Sandia National Laboratories, Livermore, CA 94551, USA*

Received 24 August 2007; received in revised form 10 October 2007; accepted 26 October 2007
Available online 17 November 2007

Abstract

The use of photoionization mass spectrometry for the development of quantitative kinetic models for the complex combustion chemistry of both conventional hydrocarbon fuels and oxygenated biofuels requires near-threshold measurements of absolute photoionization cross-sections for numerous reaction intermediates. Near-threshold absolute cross-sections for molecular and dissociative photoionization for 20 stable reaction intermediates (methane, ethane, propane, *n*-butane, cyclopropane, methylcyclopentane, 1-butene, *cis*-2-butene, isobutene, 1-pentene, cyclohexene, 3,3-dimethyl-1-butene, 1,3-hexadiene, 1,3-cyclohexadiene, methyl acetate, ethyl acetate, tetrahydrofuran, propanal, 1-butyne, 2-butyne) are presented. Previously measured total photoionization cross-sections for 9 of these molecules are in good agreement with the present results. The measurements are performed with photoionization mass spectrometry (PIMS) using a monochromated VUV synchrotron light source with an energy resolution of 40 meV (fwhm) comparable to that used for flame-sampling molecular beam PIMS studies of flame chemistry and reaction kinetics.

Keywords: Photoionization cross-section; Hydrocarbon; Photoionization mass spectrometry (PIMS); Combustion chemistry

1. Introduction

Photoionization mass spectrometry (PIMS) is used extensively for determinations of adiabatic ionization energies, photofragment appearance energies, proton affinities, ionic heats of formation and related thermochemical properties [1,2]. Mass-resolved measurements of vacuum ultraviolet (VUV) photoionization efficiency (PIE) spectra yield *relative* cross-sections for both molecular and dissociative photoionization of parent molecules. The recent use of PIMS for quantitative studies of flame chemistry [3–5] and reaction kinetics [6,7] has generated renewed interest in measurements of *absolute* photoionization cross-sections, traditionally used for fundamental studies of photo-physical processes and applications to atmospheric and astrophysical photochemistry [1,2,8,9].

The application of photoionization mass spectrometry (PIMS), using tunable monochromated synchrotron radiation for the isomer-selective detection of flame species [3,4], contributes to a better understanding of the complex reaction kinetics of the combustion of hydrocarbon and oxygenated hydrocarbon fuels. International efforts are underway to develop detailed kinetic models of reaction mechanisms responsible for the formation of polycyclic aromatics (PAH) and soot [10] and to describe observed changes in the composition of combustion byproducts when biofuels (e.g., ethanol, biodiesel) are used as replacements for, or additives with, conventional petroleum-based fuels [11–14].

Even the simplest of these combustion models typically specify hundreds of reactions contributing to the formation and destruction of several dozen key radicals and reaction intermediates. Combustion models are partially based on absolute species concentration measurements in low-pressure one-dimensional premixed laminar flames. Such direct measurements with PIMS require absolute photoionization cross-sections for all species of interest.

* Corresponding author. Tel.: +1 607 2554191; fax: +1 607 2557658.
E-mail address: tac13@cornell.edu (T.A. Cool).

1387-3806/$ – see front matter © 2007 Elsevier B.V. All rights reserved.
doi:10.1016/j.ijms.2007.10.013

Because different isomeric forms of the reaction intermediates often follow quite different reaction pathways, experimental determinations of isomeric compositions are of crucial importance in model development. Measurements of near-threshold PIE spectra, coupled with high-level electronic structure calculations of adiabatic ionization energies, can provide unambiguous identifications of individual isomers [15–19]. Because VUV–PIE measurements provide an isomer-specific distinguishing photoionization fingerprint for each molecular species, the composition of a mixture of isomers may, in favorable cases, be resolved from the PIE spectrum for the mixture when the *absolute* photoionization cross-sections for the isomeric components are known [3,17].

Reliable absolute cross-sections for near-threshold total positive ion production for several molecules of combustion interest, performed with single- [20,21] and double- [2,22–24] ionization chamber techniques, are available in the literature [8,25–32]. For many hydrocarbon and oxygenated hydrocarbon combustion intermediates, however, appearance energies for dissociative ionization are often within 1–2 eV of the adiabatic ionization energy of the parent molecule. For these cases *mass-resolved* ion detection is necessary to measure the partial cross-sections for dissociative photoionization channels [33]. Knowledge of these partial photoionization cross-sections is of particular importance in studies of flame chemistry to account for ion fragments of a given mass-to-charge (*m*/*z*) ratio that may interfere with the detection of parent-ions of the same *m*/*z* value.

In this paper, we present measurements of absolute photoionization cross-sections for 20 stable reaction intermediates, which contribute to a growing database [2,34] of critical importance for applications of PIMS to gas phase chemistry. Tabulated cross-sections for these 20 molecules are given as a supplement to this paper (see supplementary material). These results augment recently reported measurements for both stable [33] and radical [35–37] species.

2. Experimental

2.1. Apparatus

In this section we give a brief description of the experimental methods and apparatus detailed more completely elsewhere [4,33]. Near-threshold photoionization cross-sections for "target" species of interest are determined by the comparison of photo-ion signals from the target species and those of "standard" species (propene, acetylene, ethylene) with known photoionization cross-sections.

A molecular-beam time-of-flight photoionization mass spectrometer is used for the measurements. The apparatus consists of a low-pressure (9 Torr) sample reservoir ("flame chamber"), a two-stage differentially pumped molecular beam sampling system, and a 1.3 m linear time-of-flight mass spectrometer (TOFMS) with a mass resolution $m/\Delta m = 400$. It is coupled to a 3-m monochromator used to disperse synchrotron radiation at the advanced light source (ALS) of the Lawrence Berkeley National Laboratory [38]. Higher order diffraction and high-energy undulator harmonics are suppressed by passing the undulator beam through a gas filter containing 30 Torr of argon [39]. The monochromator, with a 600 lines/mm iridium-on-copper grating, delivers a dispersed photon beam, tunable over the useful range from 8 to 17 eV, with an energy resolution of 40 meV (fwhm) for the present experiments and a typical photon current of 5×10^{13} photons/s. A silicon photodiode, with its quantum efficiency (electrons/photon) calibrated at the National Institute of Standards and Technology (NIST) from 8 to 17 eV, records the variation in photon current with photon energy. It should be noted, however, that the *ratio* of detected ion signals for target and standard molecules, used for absolute cross-section measurements, is independent of the photon current. The photodiode response was needed only for short extrapolations of target molecule cross-sections beyond the range of energies of the cross-sections for the standard molecule, as discussed in Section 3 below. Photon energies are calibrated by recording mass spectra for O_2^+ photo-ions for energies ranging from 12 to 13.2 eV, an interval that contains several narrow autoionization resonances [40]. A probable uncertainty of ±15 meV is assigned to photon energies over the energy ranges of the present measurements.

Binary mixtures of the target and standard molecules are prepared in a 3.8 l stainless steel sample cylinder with a teflon coated inner surface. Nominal sample mixture compositions consist of ca. 10 Torr each of the target and standard to which 2300 Torr of argon diluent is added. The samples are allowed to mix for at least 8 h and then are introduced as a cold flow to the reservoir at a flow rate of 0.1 slm (standard liters per minute) along with a second flow of argon at 0.15 slm. The slowly flowing gas mixture in the reservoir is sampled by rapid expansion through a quartz cone with a 0.2 mm orifice diameter located on the flow axis. A skimmer of 2.0-mm-diameter aperture placed 23 mm downstream on the axis of the expanded (10^{-5} Torr) jet from the sampling cone forms a molecular beam that passes into the differentially pumped (5×10^{-7} Torr) ionization region, where it is crossed by the dispersed VUV light from the monochromator.

Photo-ions are extracted by pulse-gating the repeller plate of the TOFMS to propel the ions along the flight tube to a microchannel (MCP) detector (Burle, APD). A multichannel scaler (Fast ComTec P7886) records ion counts for a 30 μs sweep (15,008 channels of 2 ns bin width) following each gate pulse. Typically, mass spectra are recorded for 5×10^5 to 2×10^6 sweeps with a dynamic range of 10^5. The ion signal at a given mass/charge (*m*/*z*) ratio is obtained by integration of the accumulated ion counts per channel over 25–40 multiscaler channels (50–80 ns) centered at the mass peak. The total ion count is corrected for the baseline contribution obtained between peaks, the contributions of ^{13}C isotopomers, and finally normalized by the photon current.

Synchrotron PIMS studies of flame chemistry are typically performed with photon energies ranging from 7 to 17 eV, with resolutions $E/\Delta E$ (fwhm) from 250 to 1000, depending on monochromator slit widths [4,41]. Because photoionization spectra often exhibit narrow autoionization resonances, it is

important that photoionization cross-sections be measured at energy resolutions corresponding to those used for the flame chemistry [3–5] and reaction kinetics [6,7] studies.

The sources of the chemicals used in these studies are as follows: propene 99+% (Aldrich), acetylene (0.9% in 99.1% nitrogen) (Matheson), ethylene CP grade (Air Products), methane 99.99% (Matheson), ethane 99.99% (Aldrich), propane 99.97% (Aldrich), *n*-butane 99% (Aldrich), cyclopropane 99+% (Aldrich), methylcyclopentane 97% (Aldrich), 1-butene 99+% (Aldrich), *cis*-2-butene 99+% (Aldrich), isobutene 99% (Aldrich), 1-pentene 99% (Aldrich), cyclohexene 99+% (Aldrich), 3,3-dimethyl-1-butene 95% (Aldrich), 1,3-hexadiene (mixture of *cis* and *trans*) 95% (Aldrich), 1,3-cyclohexadiene 97% (Aldrich), methyl acetate 99.5% (Aldrich), ethyl acetate 99.5+% (Aldrich), tetrahydrofuran 99.9+% (Aldrich), propanal 97+% (Aldrich), 1-butyne 98+% (Aldrich), 2-butyne 99% (Aldrich).

2.2. Measurement procedure

Measurements of absolute photoionization cross-sections require that the ion detection efficiency of the apparatus be determined using calibration gases with known photoionization cross-sections. We summarize here the measurement procedures described previously in greater detail [33]. Propene is a convenient calibration standard over the photon energy range from 9.7 to 11.75 eV for which the absolute cross-sections for molecular photoionization have been accurately measured by Person and Nicole [26,42]. Propene cannot, however, be used as a calibration standard for cross-section measurements of the cyclopropane C_3H_6 isomer; in this case ethylene is used as a reliable standard. Acetylene is used as a standard for methane and ethane at higher photon energies, extending to 13.6 eV. Tabulated photoionization cross-sections for acetylene for photon energies ranging from 11.36 to 13.56 eV, and ethylene from 10.03 to 11.78 eV, used in this work are given in reference
[33].

The precision of the present measurements is reflected in the standard deviations (typically ±10%) for cross-sections measured with two or more (usually three) separately prepared samples. The calibrated response of our molecular beam TOFMS system accounts for mass discrimination effects that deplete the concentrations of molecules of light mass relative to heavier molecular beam components [43,44]. A probable error of ±10% is assigned to the mass discrimination factors (cf. Fig. 1) for parent-ions with m/z values below 70; errors as large as ±15% are possible for higher m/z. The cross-sections for propene and ethylene used as calibration standards for measurements below 11.75 eV have uncertainties of less than ±10%. Estimated uncertainties in the acetylene cross-sections used as calibration standards for methane and ethane range from ±10% below 12 eV to ±20% at 13.56 eV. An overall uncertainty of ±20% is assigned for cross-sections for all molecules except for methane and ethane, which may have uncertainties of ±25% at the highest photon energies.

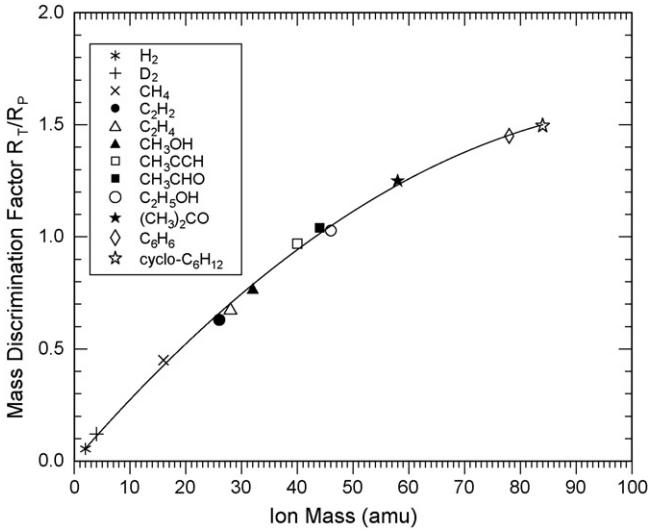

Fig. 1. The symbols are the mass discrimination factors R_T/R_P relative to propene cf. Eq. (1) for 11 specified target species. The solid curve is a fit to the 11 data points used to obtain mass discrimination factors for cross-section measurements for other molecules reported here.

The ratio of target ion signal to standard ion signal is given by the relationship [4,45]:

$$\frac{S_T}{S_S} = \left[\frac{R_T}{R_S}\right]\left[\frac{\sigma_T(E)}{\sigma_S(E)}\right]\left[\frac{P_T}{P_S}\right] \quad (1)$$

Here P_T/P_S is the ratio of target gas to standard gas partial pressures in the binary gas mixture, $\sigma_T(E)/\sigma_S(E)$ is the ratio of target to standard photoionization cross-sections at the photon energy E, and R_T and R_S are mass-dependent response factors that account for differing sampling and detection efficiencies for the target and standard ions.

The ratios R_T/R_S "mass discrimination factors" [46] for our apparatus are displayed in Fig. 1. According to Eq. (1), the ratio of recorded ion signals at the photon energy E for a given target molecule to that of a standard molecule, S_T/S_S, is directly proportional to the mass discrimination factor multiplied by the product of the ratio of photoionization cross-sections, $\sigma_T(E)/\sigma_S(E)$, and the corresponding ratio of partial pressures. Measurements of the ratio of target ion signal to that of propene, recorded for binary mixtures of 11 target molecules with propene, were used to construct Fig. 1. The symbols indicate the mass discrimination factors R_T/R_P relative to propene ($m/z = 42$) calculated with Eq. (1) for each of the 11 specified target species. The solid curve is a fit to these data used to obtain mass discrimination factors for cross-section measurements for other molecules reported here.

3. Results

We present here near-threshold absolute photoionization cross-sections for 20 molecules based on the use of Eq. (1) and the mass discrimination factors (fitted curve) of Fig. 1. The error limits of the measurements shown with the data for a few representative photon energies are the ±1 standard deviations for two to three separately prepared target/standard mixtures.

Table 1
The first and second ionization energies

Molecules	Adiabatic ionization energy [47]	Second IE	
		Vertical	Adiabatic
Methane	12.61	14.4 [59]	
Ethane	11.52	12.7 [59]	
Propane	10.94	12.1 [59]	
n-Butane	10.53	11.7 [59]	
Cyclopropane	9.86	11.3 [59]	
Methylcyclopentane	9.7		
1-Butene	9.55		11.30 [54]
cis-2-Butene	9.11	11.65 [67]	11.28 [54]
Isobutene	9.22	11.8 [59]	11.36 [54]
1-Pentene	9.49	11.37 [58]	10.82 [58]
3,3-Dimethyl-1-butene	9.45	11.2 [68]	10.5 [68]
Cyclohexene	8.94	11.6 [67]	10.3 [67]
1,3-Hexadiene	8.52	10.94 [69]	10.6 [69]
1,3-Cyclohexadiene	8.25	10.7 [59,67]	10.5 [67]
Methyl acetate	10.25	11.16 [61]	
Ethyl acetate	10.01	10.99 [61]	
Tetrahydrofuran	9.40	11.52 [67]	11.1 [67]
Propanal	9.96	12.62 [67]	11.75 [67]
1-Butyne	10.18	10.3 [59]	
2-Butyne	9.58	14.3 [59]	

The adiabatic ionization energies and second ionization energies for the molecules of this study are listed in Table 1. In this paper quoted values for appearance energies for dissociative ionization channels are taken from reference [47]. Some target molecules (1-butene, *cis*-2-butene, isobutene, 1-pentene, 3,3-dimethyl-1-butene, cyclohexene, 2-butyne, 1,3-hexadiene, 1,3-cyclohexadiene and tetrahydrofuran) have adiabatic ionization energies below that of propene at 9.73 eV [47]. For these molecules the measured ion signals, corrected for changes in photon current with photon energy, were used to extrapolate cross-sections to threshold. A similar procedure was followed for cyclopropane with an ionization energy of 9.86 eV, below that (10.51 eV) of the ethylene calibration standard. The photon-current-corrected ion signals for methane and propane were also used to extend their cross-section measurements to 14.09 and 12.49 eV, respectively.

For propane, *n*-butane, and methylcyclopentane measurements of the partial cross-sections for $C_3H_6^+$ and $C_3H_7^+$ required supplemental observations of these two fragment ions in the absence of admixed propene. The contribution of ^{13}C isotopomers of $C_3H_6^+$ is subtracted from the $C_3H_7^+$ ion signal to obtain the $C_3H_7^+$ cross-section. Similarly, the cross-sections for dissociative ionization leading to $C_3H_6^+$ fragment ions for 1-pentene and tetrahydrofuran required measurements for 1-pentene/argon and tetrahydrofuran/argon mixtures with no admixed propene.

3.1. Methane, ethane, propane, n-butane, cyclopropane, methylcyclopentane

The total photoionization cross-sections for all six alkanes of the present study and those for cyclohexane reported previously [33] rise monotonically above threshold in a quasi-linear fashion in agreement with qualitative expectations discussed by Koizumi [48]. Fig. 2 shows absolute photoionization cross-sections for methane for photon energies from 12.54 to 14.09 eV, using acetylene as the calibration standard. No fragmentation is observed over this energy range. Our measurements are compared with previous results of Samson et al. [27], Backx et al. [49] and Kameta et al. [28]. The present measurements are in reasonable agreement with the accurate photoionization cross-sections measured by Samson et al. using a double ionization chamber and an argon discharge lamp. The measurements of Kameta et al. with a double ionization chamber and monochromated synchrotron radiation are about 10–15% lower than our data, while the measurements of Backx et al., who used the equivalent dipole electron-ion coincidence (e, e, +ion) method, lie above our values near threshold.

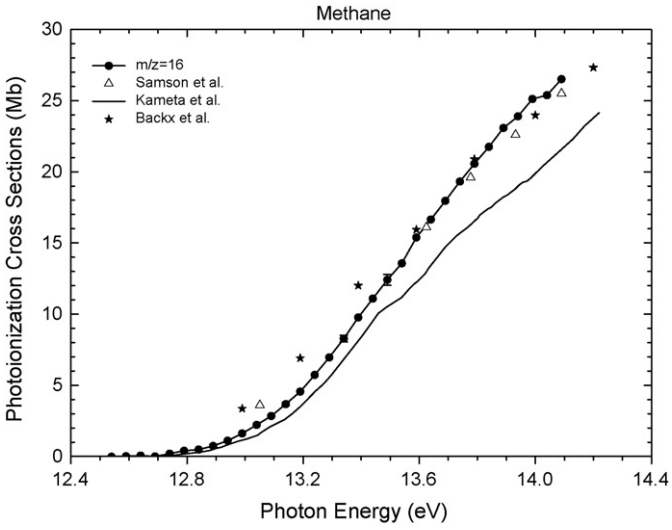

Fig. 2. Absolute cross-sections for the photoionization of methane. The present results are compared with the previous measurements of Samson et al. [27], Kameta et al. [28], and Backx et al. [49].

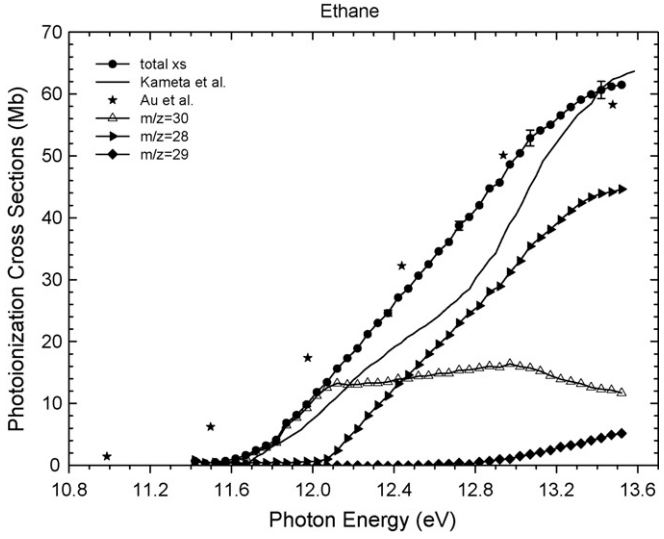

Fig. 3. Molecular and dissociative photoionization cross-sections for ethane. The total photoionization cross-sections are compared with the previous measurements of Kameta et al. [29] and Au et al. [51,52].

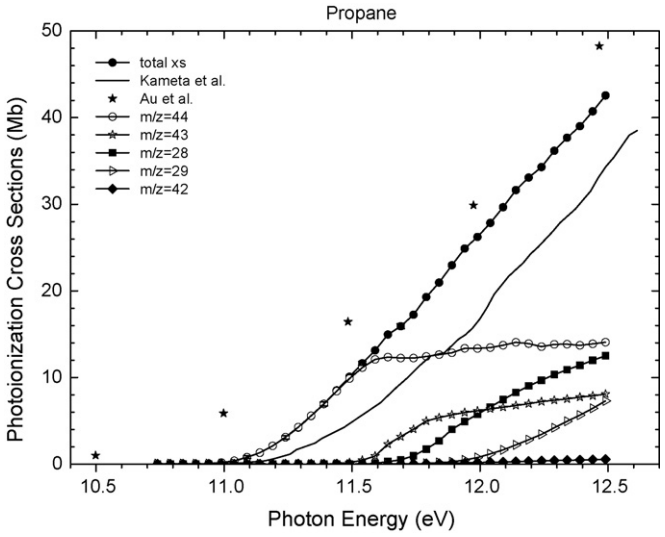

Fig. 4. Molecular and dissociative photoionization cross-sections for propane. The total photoionization cross-sections are compared with the previous measurements of Kameta et al. [29] and Au et al. [51,52].

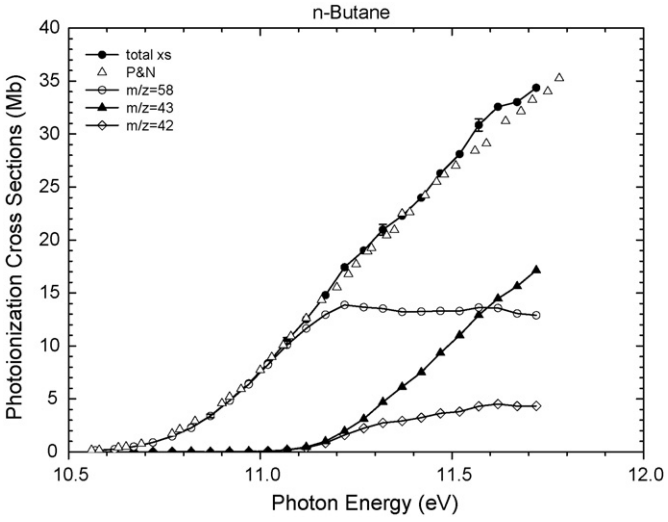

Fig. 5. Molecular and dissociative photoionization cross-sections for *n*-butane. The total photoionization cross-sections are compared with the previous measurements of Person and Nicole [25].

Fragmentation is observed for ethane and propane for photon energies 1–2 eV above their molecular ionization thresholds, as illustrated in Figs. 3 and 4. For ethane, the fragment ion $C_2H_4^+$ ($m/z = 28$) with an appearance energy near 12.1 eV contributes substantially to the total photoionization cross-section at higher energies. The fragment ion $C_2H_5^+$ ($m/z = 29$) appears near 12.4 eV with a cross-section much smaller than that of the $C_2H_4^+$ dissociative fragment.

For propane, the prominent fragment ions observed below 12.5 eV are $C_3H_7^+$ ($m/z = 43$), $C_2H_4^+$ ($m/z = 28$) and $C_2H_5^+$ ($m/z = 29$), with appearance energies of 11.59, 11.69 and 11.90 eV [47], respectively. The fragment ion $C_3H_6^+$ ($m/z = 42$) only makes a small contribution to the total cross-section. Our total and partial cross-section measurements of Figs. 3 and 4 are in good qualitative agreement with the photoionization efficiency curves for ethane and propane reported by Chupka and Berkowitz [50]. The total cross-sections for ethane and propane are compared with the results of Kameta et al. [29] and Au et al. [51,52]. Here again the results of Kameta et al. are lower than our data. The poor energy resolution (1 eV) of the dipole (e, e, +ion) measurements of Au et al. accounts for the anomalous shifts in their ionization thresholds to lower energies.

The total cross-sections for *n*-butane shown in Fig. 5 are in excellent agreement with the accurate measurements of Person and Nicole [25]. The fragment ions $C_3H_7^+$ ($m/z = 43$) and $C_3H_6^+$ ($m/z = 42$) appear at almost the same energy near 11.05 eV [47]. Our measurements for *n*-butane are also in good agreement with the relative cross-sections obtained by Chupka and Berkowitz [50].

Fig. 6 presents absolute photoionization cross-sections for cyclopropane for photon energies ranging from 9.64 to 11.74 eV obtained with Eq. (1) using ethylene as the standard. A small contribution from the fragment ion $C_3H_5^+$ ($m/z = 41$) is present above 11.5 eV. The total cross-sections agree very well with the previous measurements of Koizumi and co-workers [31,32], performed with a double ionization chamber and monochromated synchrotron radiation. The measurements reported by Kameta et al. [30] lie consistently below our data, as was the case for methane, ethane and propane.

The cross-sections for methylcyclopentane of Fig. 7 provide an interesting comparison with those measured previously [33] for the cyclohexane C_6H_{12} isomer. Despite their structural differences, the major dissociative ionization channels are $C_4H_8^+$ ($m/z = 56$) + C_2H_4 and $C_5H_9^+$ ($m/z = 69$) + CH_3 for both molecules. No previous studies of the photoionization of methylcyclopentane have been reported, but the appearance energy for the $C_5H_9^+$ dissociative photoionization fragment of Fig. 7 is in good agreement with the electron ionization value of 10.73 eV reported by Lossing and Traeger [53].

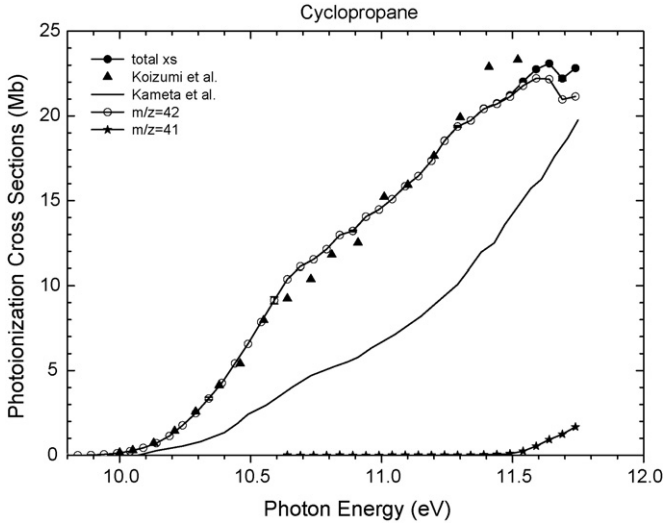

Fig. 6. Molecular and dissociative photoionization cross-sections for cyclopropane. The total photoionization cross-sections are compared with the previous measurements of Koizumi et al. [31,32] and Kameta et al. [30].

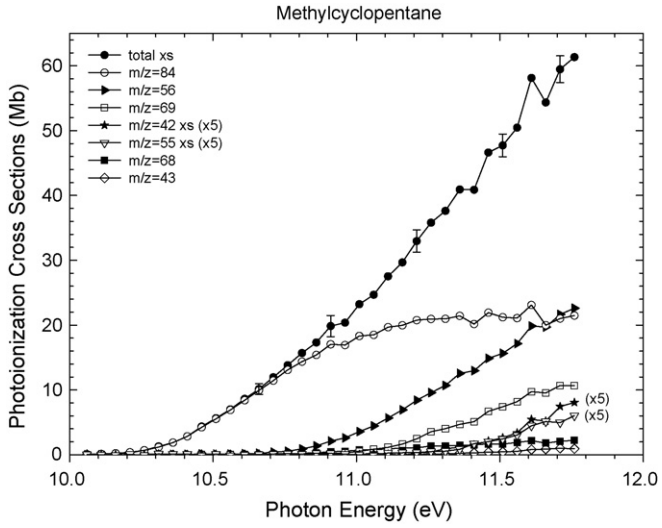

Fig. 7. Molecular and dissociative photoionization cross-sections for methylcyclopentane.

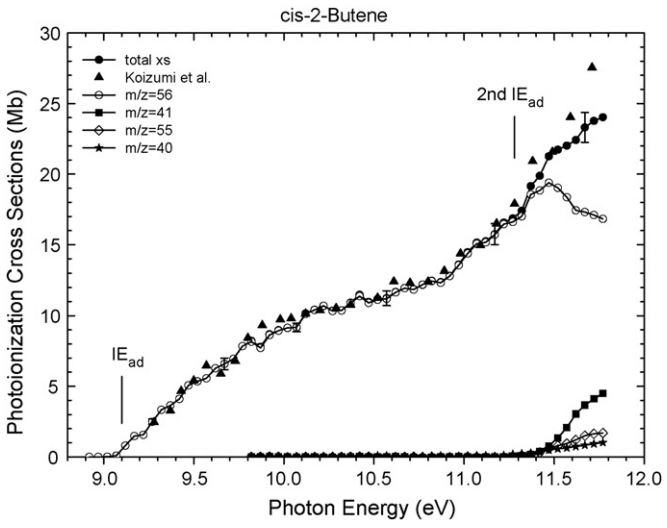

Fig. 9. Molecular and dissociative photoionization cross-sections for *cis*-2-butene. The total photoionization cross-sections are compared with the previous measurements of Koizumi et al. [31,32].

3.2. 1-Butene, cis-2-butene, isobutene, 1-pentene, cyclohexene and 3,3-dimethylbutene

The photoionization cross-sections for the six alkenes presented here exhibit similarities in common with other monounsaturated alkenes, including the cross-sections for *cis*-2-pentene, *trans*-2-pentene, and cyclopentene reported previously [33]. The lowest ionization energy corresponds to the removal of an electron from a π orbital of the C=C double bond. The energy separating the first and second ionization energies is often large enough that, in the absence of pronounced vibrational structure and autoionization features, a clearly defined plateau in the PIE curves, corresponding to photoionization cross-sections ca. 10–15 Mb (1 Mb = 10^{-18} cm^2), is reached just above threshold, extending to the second ionization energy [48]. Dissociative ionization channels typically appear for photon energies in the vicinity of the adiabatic second ionization energy of the parent-ion.

For 1-butene (Fig. 8) and *cis*-2-butene (Fig. 9), much of the rapid increase in total photoionization cross-sections beyond the respective adiabatic second ionization energies of 11.30 and 11.28 eV [54] results from the opening of dissociative photoionization channels leading to three fragment ions $C_4H_7^+$ ($m/z = 55$), $C_3H_5^+$ ($m/z = 41$) and $C_3H_4^+$ ($m/z = 40$). The parent-ion cross-sections for 1-butene and *cis*-2-butene are in good qualitative agreement with the photoionization efficiency curves recorded by Wood and Taylor [55].

The total photoionization cross-section for isobutene (Fig. 10) beyond the second ionization energy (11.36 eV) [54] rises more slowly and the cross-sections for the three fragment ions are much smaller than for 1-butene and *cis*-2-butene.

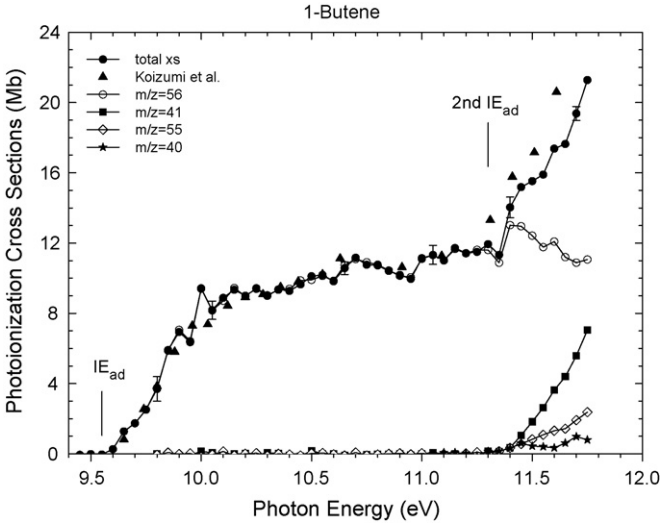

Fig. 8. Molecular and dissociative photoionization cross-sections for 1-butene. The total photoionization cross-sections are compared with the previous measurements of Koizumi et al. [31,32].

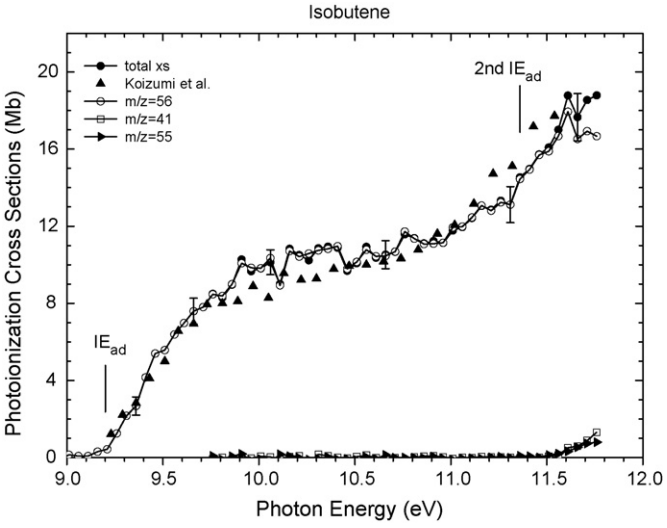

Fig. 10. Molecular and dissociative photoionization cross-sections for isobutene. The total photoionization cross-sections are compared with the previous measurements of Koizumi et al. [31,32].

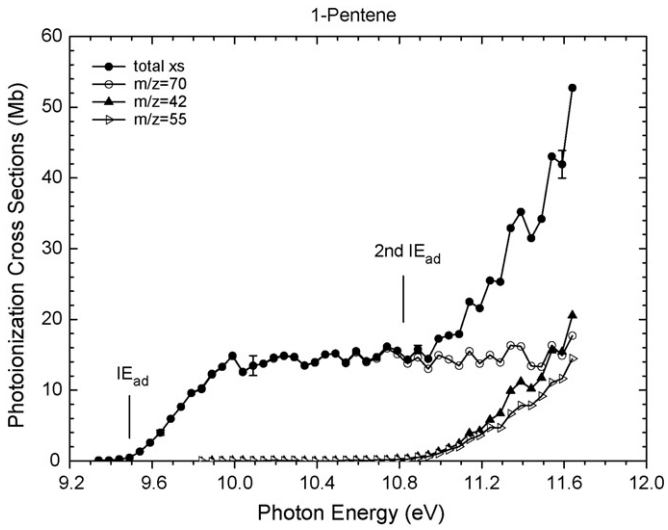

Fig. 11. Molecular and dissociative photoionization cross-sections for 1-pentene.

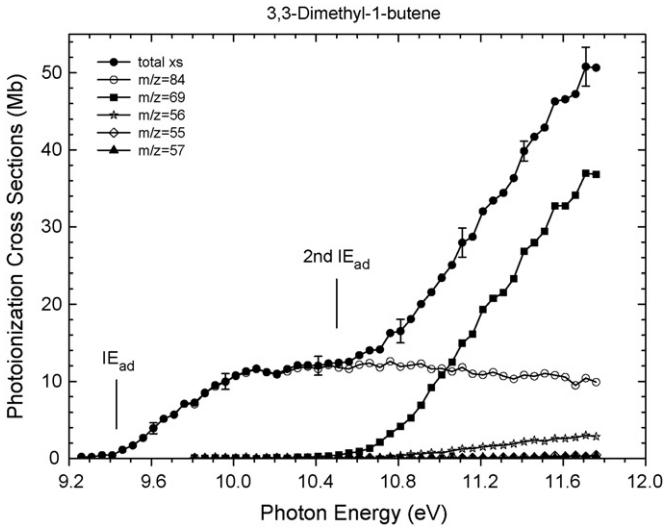

Fig. 13. Molecular and dissociative photoionization cross-sections for 3,3-dimethyl-1-butene.

Indeed, the $C_3H_4^+$ ($m/z = 40$) ion signal is barely discernable above the background and is not shown in Fig. 10. The total cross-sections for 1-butene, *cis*-2-butene, and isobutene are in excellent agreement with the measurements of Koizumi et al. [31,32].

Fig. 11 displays the photoionization cross-sections for 1-pentene. The parent-ion cross-section rises smoothly from threshold at 9.49 eV to reach a plateau near 10 eV extending to the 11.64 eV limit of the present measurements. The dissociative ionization channels for $C_3H_6^+$ ($m/z = 42$) and $C_4H_7^+$ ($m/z = 55$) open [56,57] just below the 10.82 eV second ionization energy [58].

The total ionization cross-section for cyclohexene (Fig. 12) rises smoothly from threshold at 8.95 eV, reaches a plateau and then rapidly increases above 10.3 eV with the appearance of the dissociative ionization channel leading to the major fragment ion $C_5H_7^+$ ($m/z = 67$) and CH_3. The other two fragment ions $C_4H_6^+$ ($m/z = 54$) and $C_6H_9^+$ ($m/z = 81$) only make small contributions to the total cross-section.

The cross-sections for 3,3-dimethyl-1-butene (Fig. 13) are qualitatively similar to those for cyclohexene. Here again the total ionization cross-section rises smoothly from threshold at 9.45 eV, reaches a plateau, and exhibits a marked increase as the major fragmentation channel leading to $C_5H_9^+$ and CH_3 opens above 10.5 eV. Three other fragment ions $C_4H_8^+$ ($m/z = 56$), $C_4H_7^+$ ($m/z = 55$) and $C_4H_9^+$ ($m/z = 57$) also appear, but make only minor contributions to the total ionization cross-section.

3.3. 1,3-Hexadiene and 1,3-cyclohexadiene

Fig. 14 presents the photoionization cross-sections for 1,3-hexadiene. The parent-ion cross-section for 1,3-hexadiene rises

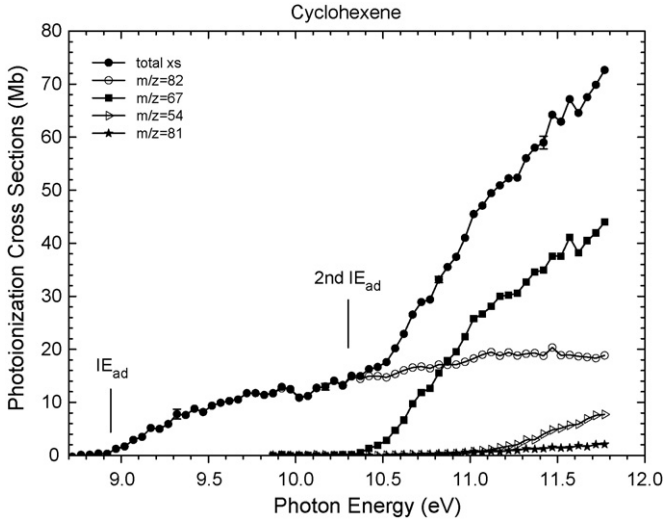

Fig. 12. Molecular and dissociative photoionization cross-sections for cyclohexene.

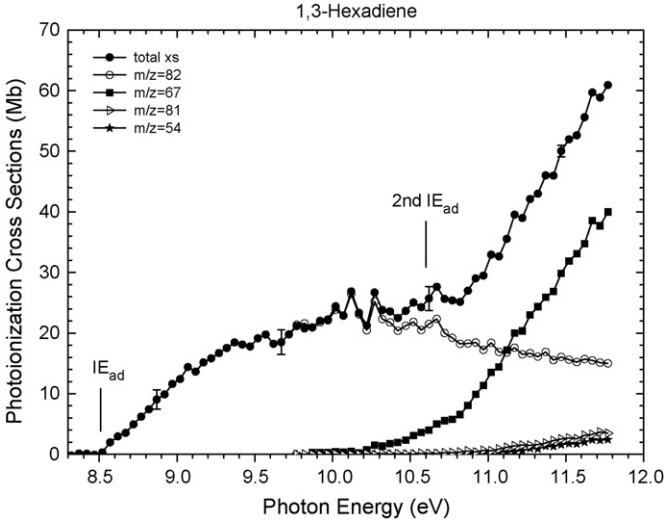

Fig. 14. Molecular and dissociative photoionization cross-sections for 1,3-hexadiene.

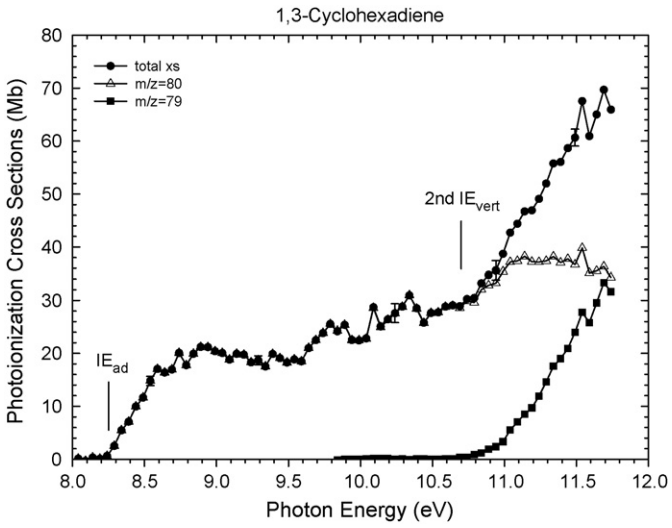

Fig. 15. Molecular and dissociative photoionization cross-sections for 1,3-cyclohexadiene.

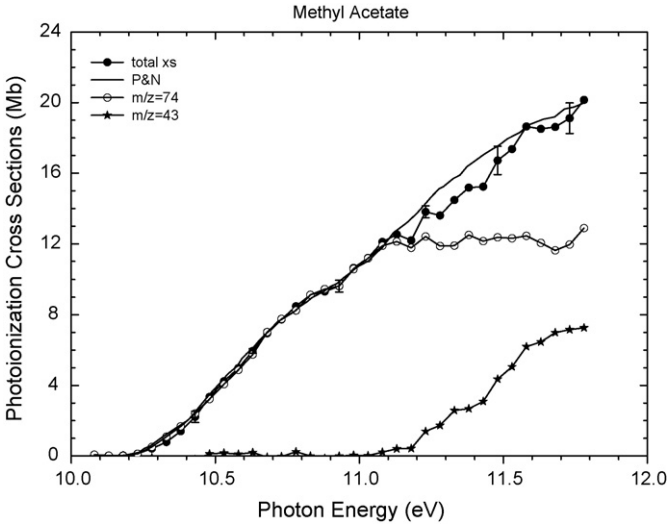

Fig. 16. Molecular and dissociative photoionization cross-sections for methyl acetate. The total photoionization cross-section is compared with the previous measurements of Person and Nicole [26].

smoothly from threshold at 8.54 eV [47], reaches a maximum of 26.4 Mb at 10.12 eV, the appearance energy for the major fragment ion $C_5H_7^+$ ($m/z = 67$), and then slowly decreases in competition with the dissociative ionization channels. The minor fragment ions $C_6H_9^+$ ($m/z = 81$) and $C_4H_6^+$ ($m/z = 54$) make small contributions to the total cross-section. Comparison with the cross-sections for cyclohexene (cf. Fig. 12) reveals a marked similarity between cross-sections for the two isomers.

The 1,3-cyclohexadiene photoionization cross-sections for parent $C_6H_8^+$ ($m/z = 80$) and fragment $C_6H_7^+$ ($m/z = 79$) ions are presented in Fig. 15. The parent-ion cross-section rises from threshold at 8.25 eV [47] to reach a plateau of ca. 20 Mb before the onset of dissociative ionization near 10.7 eV. The $C_6H_7^+$ fragment ion and total ionization cross-sections rise steeply beyond the second ionization energy at 10.7 eV [59]. No previous cross-section measurements are available for 1,3-hexadiene and 1,3-cyclohexadiene.

3.4. Methyl acetate and ethyl acetate

Clean-burning renewable biodiesel fuels are of potential importance as additives to, or replacements for, conventional gasoline and diesel fuels, which may reduce dependence on imported petroleum and lower net greenhouse-gas emissions. PIMS measurements of the composition of reaction intermediates are needed for the development of appropriate models for the combustion chemistry of methyl and ethyl esters, typical constituents of biodiesel fuels [60]. The lowest ionization energies for the methyl and ethyl esters of acetic acid, model representatives for biodiesel compounds, correspond to the removal of an electron from the carbonyl oxygen lone-pair orbital, while the second ionization energy originates from a nonbonding π orbital of predominantly lone-pair character centered on the oxygen atom of the ester group, as discussed by Sweigart and Turner [61]. The near-threshold parent-ion photoionization cross-sections for methyl and ethyl acetate are shown in Figs. 16 and 17. For both molecules the total photoionization cross-sections rise from threshold in a quasi-linear fashion for photon energies extending to the limits of the present measurements. The parent-ion cross-sections reach an extensive plateau with the onset of dissociative ionization. The total photoionization cross-section for methyl acetate is in excellent agreement with the measurements of Person and Nicole [26], no previous measurements of ionization cross-sections for ethyl acetate are available.

For methyl acetate the CH_3CO^+ ($m/z = 43$) acetyl cation is the only fragment ion observed below 11.78 eV with an appearance energy near 11.05 eV in excellent agreement with the measurements of Traeger et al. [62]. Ethyl acetate exhibits extensive fragmentation beyond 10.4 eV yielding $C_4H_6O^+$ ($m/z = 70$),

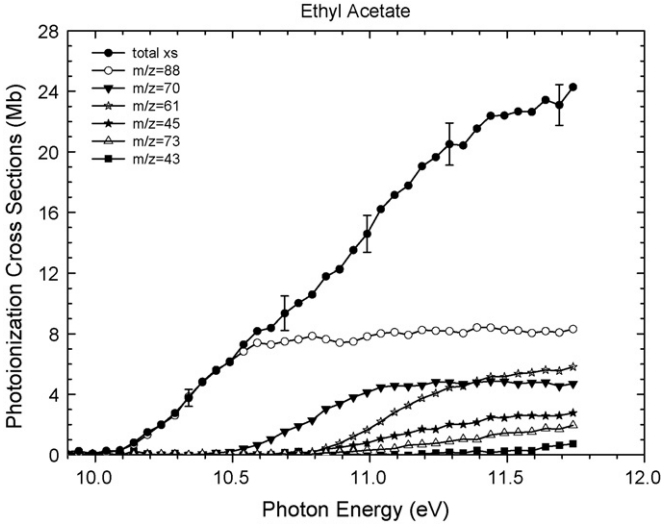

Fig. 17. Molecular and dissociative photoionization cross-sections for ethyl acetate.

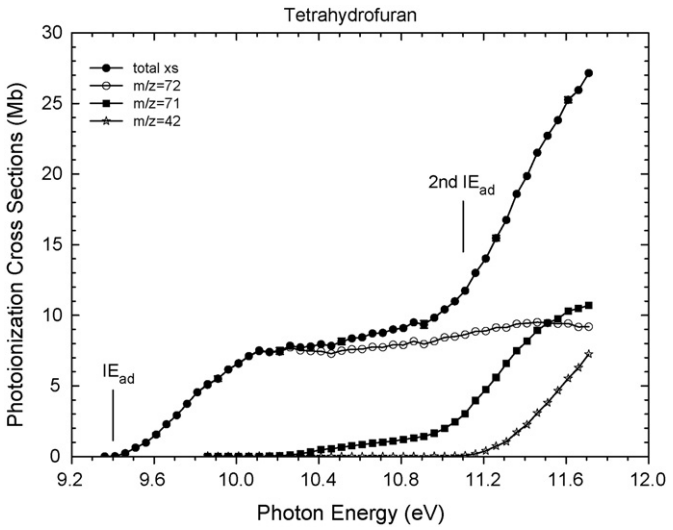

Fig. 18. Molecular and dissociative photoionization cross-sections for tetrahydrofuran.

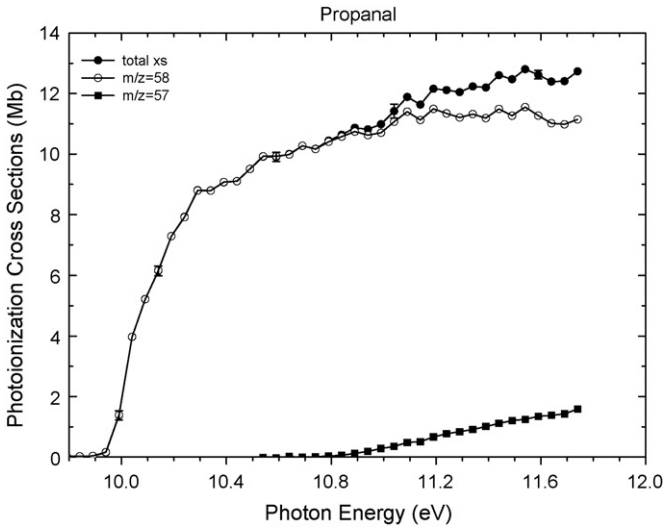

Fig. 19. Molecular and dissociative photoionization cross-sections for propanal.

$C_2H_5O_2^+$ ($m/z = 61$), $C_2H_5O^+$ ($m/z = 45$), $C_3H_5O_2^+$ ($m/z = 73$), and $C_2H_3O^+$ ($m/z = 43$). Appearance energies for these fragments are given in reference [47]. The photoelectron bands observed for the first and second ionization energies for both methyl acetate and ethyl acetate are quite broad [61], making estimates of the adiabatic second ionization energies difficult, cf. Table 1.

3.5. Tetrahydrofuran

The lowest ionization energy for ethers arises from the removal of an electron from a lone-pair orbital centered on the oxygen atom [48,63]. Neglecting the possible effects of conjugation, the near-threshold photoionization cross-sections are not expected to be strongly influenced by the hydrocarbon structures of the parent molecules. This is illustrated for the parent-ion photoionization cross-section presented in Fig. 18 for the cyclic ether, tetrahydrofuran, which is quite similar to those for simple non-cyclic ethers [33,48]. The parent-ion cross-section for tetrahydrofuran increases smoothly from threshold at 9.40 eV to reach a plateau at 10.2 eV, near the appearance energy [47] for the $C_4H_7O^+$ ($m/z = 71$) fragment ion, but well below the appearance of the $C_3H_6^+$ ($m/z = 42$) fragment at the 11.1 eV estimated adiabatic second ionization energy.

3.6. Propanal

The lowest ionization energies of simple aldehydes correspond to the removal of a nonbonding electron from the carbonyl oxygen [64]. The parent-ion cross-section for propanal (Fig. 19) rises smoothly from threshold at 9.96 eV [47] to reach a plateau of similar shape and magnitude to that observed for acetaldehyde [26], and those seen for ethers and esters, which also originate from photoionization from oxygen lone-pair π orbitals. The $C_3H_5O^+$ ($m/z = 57$) fragment ion makes a small contribution to the total cross-section above 10.79 eV [65].

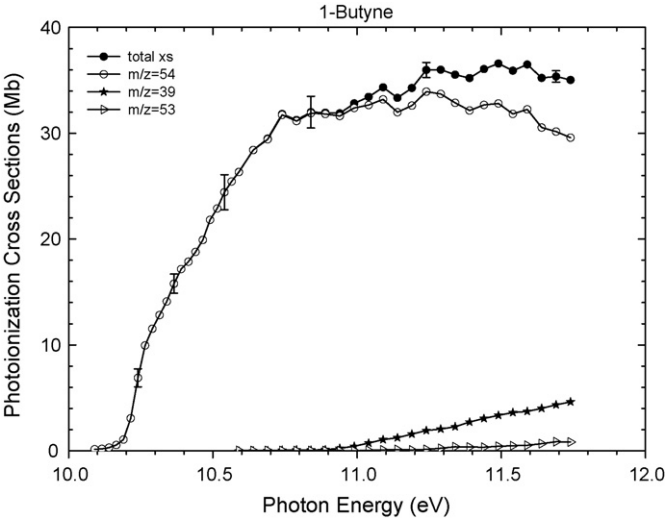

Fig. 20. Molecular and dissociative photoionization cross-sections for 1-butyne.

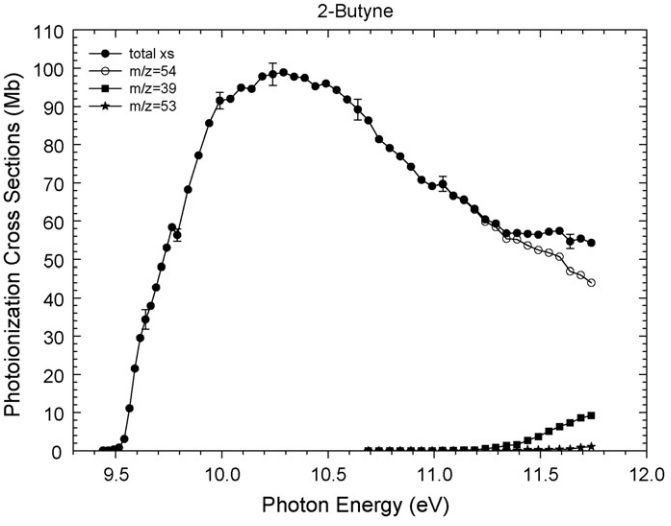

Fig. 21. Molecular and dissociative photoionization cross-sections for 2-butyne.

3.7. 1-Butyne and 2-butyne

The near-threshold photoionization cross-sections, presented in Figs. 20 and 21for 1-butyne and 2-butyne have very different magnitudes. The cross-section for the parent-ion ($m/z = 54$) for 1-butyne rises smoothly from threshold at 10.18 eV, reaches a maximum value ca. 33.9 Mb near 11.24 eV and then decreases very slowly to 29.6 Mb at the 11.74 eV limit of the present measurements. The major fragment ion $C_3H_3^+$ ($m/z = 39$) appears near 10.9 eV; the $C_4H_5^+$ ($m/z = 53$) fragment ion makes only a small contribution to the total cross-section. For 2-butyne, the parent cross-section rises steeply from threshold, reaches a maximum at 10.29 eV of 98.9 Mb, nearly 3 times larger than the maximum cross-section for 1-butyne. The parent cross-section decreases rapidly to ca. 42 Mb at 11.74 eV. Here again the major fragment ion is $C_3H_3^+$, which appears at 11.04 eV [47]. The total cross-section for 1-butyne is qualitatively similar to the photoionization coefficient measured by Nakayama and Watanabe [66]. No previous cross-section measurements for 1-butyne and 2-butyne have been reported.

The lowest ionization energy of 2-butyne results from the removal of an electron from the degenerate π orbital associated with its D_{3h} structure [59]. In contrast, for 1-butyne the lowest ionization energy arises from the removal of an electron from a nondegenerate π orbital of its low-symmetry C_S structure [59]. Structural differences evidently exert a complex influence on the magnitudes of the cross-sections for these two alkynes.

4. Conclusion

The qualitative behaviors of the near-threshold parent-ion photoionization cross-sections presented here and in references [33,48] for alkanes, alkenes, ethers, esters, alcohols and aldehydes are in general agreement with expectations [48]. For the alkanes, a series of closely spaced ionization energies contribute to the cross-sections above threshold. These superimposed contributions yield cross-sections that rise slowly from threshold in a quasi-linear fashion (cf. Figs. 2–7).

For monounsaturated alkenes (cf. Figs. 8–13), the energy separating the first and second ionization energies is large enough that, in the absence of pronounced vibrational structure and autoionization features, a clearly defined plateau in the PIE curves is reached just above threshold, extending to the second ionization energy [48]. The cross-sections for the dienes, 1,3-hexadiene (Fig. 14) and 1,3-cyclohexadiene (Fig. 15), exhibit a similar behavior with cross-section values at the plateaus roughly twice as large as observed for the monounsaturated alkenes. On the other hand, the cross-sections at the plateau for 1,3-butadiene [33] are comparable to those seen for the monounsaturated alkenes.

The parent-ion cross-sections between the first and second ionization energies for methyl acetate (Fig. 16), ethyl acetate (Fig. 17), tetrahydrofuran (Fig. 18), and propanal (Fig. 19) are similar in appearance to those seen for the monounsaturated alkenes. This feature reflects the fact that the first ionization energies corresponding to the removal of an oxygen lone-pair electron are well separated in energy from the second ionization energies.

The near-threshold photoionization cross-sections for 1-butyne (Fig. 20), 2-butyne (Fig. 21), acetylene [33], diacetylene [33], and vinylacetylene [33] exhibit complexities corresponding to marked differences in electronic structures.

As a result the near-threshold parent-ion cross-sections for these alkynes do not exhibit pronounced generic characteristics, in contrast to the monounsaturated alkenes, ethers, esters, aldehydes and alcohols [48].

The photoionization cross-sections presented here are given in tabular form in the supplementary data to this paper. The development and testing of comprehensive kinetic models of combustion chemistry will require measurements of photoionization cross-sections for many additional stable and radical intermediate species.

Acknowledgements

The authors are grateful to Paul Fugazzi for expert technical assistance. This work is supported by the Division of Chemical Sciences, Geosciences, and Biosciences, the Office of Basic Energy Sciences, the U.S. Department of Energy, in part under grant DE-FG02-01ER15180 and by the Chemical Sciences Division of the U.S. Army Research Office. Sandia is a multi-program laboratory operated by Sandia Corporation, a Lockheed Martin Company, for the National Nuclear Security Administration under contract DE-AC04-94-AL85000. The Advanced Light Source is supported by the Director, Office of Science, Office of Basic Energy Sciences, Materials Sciences Division, of the U.S. Department of Energy under contract no. DE-AC02-05CH11231 at Lawrence Berkeley National Laboratory.

Appendix A. Supplementary data

Supplementary data associated with this article can be found, in the online version, at doi:10.1016/j.ijms.2007.10.013.

References

[1] S.G. Lias, J.E. Bartmess, J.F. Liebman, J.L. Holmes, R.D. Levin, W.G. Mallard, J. Phys. Chem. Ref. Data 17 (Suppl. 1) (1988) 1.
[2] J.W. Gallagher, C.E. Brion, J.A.R. Samson, P.W. Langhoff, J. Phys. Chem. Ref. Data 17 (1988) 9.
[3] T.A. Cool, K. Nakajima, T.A. Mostefaoui, F. Qi, A. Mcllroy, P.R. Westmoreland, M.E. Law, L. Poisson, D.S. Peterka, M. Ahmed, J. Chem. Phys. 119 (2003) 8356.
[4] T.A. Cool, A. Mcllroy, F. Qi, P.R. Westmoreland, L. Poisson, D.S. Peterka, M. Ahmed, Rev. Sci. Instrum. 76 (2005) 094102.
[5] C.A. Taatjes, N. Hansen, A. McIlroy, J.A. Miller, J.P. Senosiain, S.J. Klippenstein, F. Qi, L. Sheng, Y. Zhang, T.A. Cool, J. Wang, P.R. Westmoreland, M.E. Law, T. Kasper, K. Kohse-Höinghaus, Science 308 (2005) 1887.
[6] G. Meloni, P. Zou, S.J. Klippenstein, M. Ahmed, S.R. Leone, C.A. Taatjes, D.L. Osborn, J. Am. Chem. Soc. 128 (2006) 13559.
[7] F. Goulay, D.L. Osborn, C.A. Taatjes, P. Zou, G. Meloni, S.R. Leone, Phys. Chem. Chem. Phys. 31 (2007) 4291.
[8] J. Berkowitz, Photoabsorption, Photoionization and Photoelectron Spectroscopy, Academic Press, New York, 1979.

[9] J. Berkowitz, Atomic and Molecular Photoabsorption, Absolute Total Cross Sections, Academic Press, New York, 2002.
[10] C.S. McEnally, L.D. Pfefferle, B. Atakan, K. Kohse-Höinghaus, Prog. Energy Combust. Sci. 32 (2006) 247.
[11] M.S. Graboski, R.L. McCormick, Prog. Energy Combust. Sci. 24 (1998) 125.
[12] R.J. Crookes, Biomass Bioenergy 30 (2006) 461.
[13] C.K. Westbrook, W.J. Pitz, H.J. Curran, J. Phys. Chem. A 110 (2006) 6912.
[14] A. Demirbas, Prog. Energy Combust. Sci. 33 (2007) 1.
[15] N. Hansen, S.J. Klippenstein, C.A. Taatjes, J.A. Miller, J. Wang, T.A. Cool, B. Yang, R. Yang, L. Wei, C. Huang, J. Wang, F. Qi, M.E. Law, P.R. Westmoreland, J. Phys. Chem. A 110 (2006) 3670.
[16] N. Hansen, S.J. Klippenstein, J.A. Miller, J. Wang, T.A. Cool, M.E. Law, P.R. Westmoreland, T. Kasper, K. Kohse-Höinghaus, J. Phys. Chem. A 110 (2006) 4376.
[17] N. Hansen, T. Kasper, S.J. Klippenstein, P.R. Westmoreland, M.E. Law, C.A. Taatjes, K. Kohse-Höinghaus, J. Wang, T.A. Cool, J. Phys. Chem. A 111 (2007) 4081.
[18] N. Hansen, J.A. Miller, C.A. Taatjes, J. Wang, T.A. Cool, M.E. Law, P.R. Westmoreland, Proc. Combust. Inst. 31 (2007) 1157.
[19] N. Hansen, S.J. Klippenstein, P.R. Westmoreland, T. Kasper, K. Kohse-Höinghaus, J. Wang, T.A. Cool, Phys. Chem. Chem. Phys. (2007), doi:10.1039/b711578D.
[20] J.C. Person, P.P. Nicole, in Argonne National Laboratory Radiological Physics Division Annual Report, July 1967–June 1968, p. 105.
[21] K. Watanabe, F.M. Matsunaga, H. Sakai, Appl. Opt. 6 (1967) 391.
[22] J.A.R. Samson, L. Yin, J. Opt. Soc. Am. B 6 (1989) 2326.
[23] J.A.R. Samson, J. Opt. Soc. Am. 54 (1964) 6.
[24] N. Wainfan, W.C. Walker, G.L. Weissler, J. Appl. Phys. 24 (1953) 1318.
[25] J.C. Person, P.P. Nicole, J. Chem. Phys. 49 (1968) 5421.
[26] J.C. Person, P.P. Nicole, in Argonne National Laboratory Radiological Physics Division Annual Report, July 1969–June 1970, p. 97.
[27] J.A.R. Samson, G.N. Haddad, T. Masuoka, P.N. Paree, D.A.L. Kilcoyne, J. Chem. Phys. 90 (1989) 6925.
[28] K. Kameta, N. Kouchi, M. Ukai, Y. Hatano, J. Electron Spectrosc. Relat. Phenom. 123 (2002) 225.
[29] K. Kameta, S. Machida, M. Kitajima, M. Ukai, N. Kouchi, Y. Hatano, K. Ito, J. Electron Spectrosc. Relat. Phenom. 79 (1996) 391.
[30] K. Kameta, K. Muramatsu, S. Machida, N. Kouchi, Y. Hatano, J. Phys. B: At. Mol. Opt. Phys. 32 (1999) 2719.
[31] H. Koizumi, T. Yoshimi, K. Hironaka, S. Arai, M. Ukai, M. Morita, H. Nakazawa, A. Kimura, Y. Hatano, Y. Ito, Y. Zhang, A. Yagishita, K. Ito, K. Tanaka, Radiat. Phys. Chem. 32 (1988) 111.
[32] H. Koizumi, T. Yoshimi, K. Shinsaka, M. Ukai, M. Morita, Y. Hatano, A. Yagishita, K. Ito, K. Tanaka, J. Chem. Phys. 82 (1985) 4856.
[33] T.A. Cool, J. Wang, K. Nakajima, C.A. Taatjes, A. Mcllroy, Int. J. Mass Spectrom. 247 (2005) 18.
[34] A repository for photoionization cross section data has been established within the Collaboratory for Multi-scale Chemical Sciences (CMCS) at the Sandia National Laboratories: http://cmcs.org/technical.php.
[35] N.E. Sveum, S.J. Goncher, D.M. Neumark, Phys. Chem. Chem. Phys. 8 (2006) 592.
[36] J.C. Robinson, N.E. Sveum, D.M. Neumark, Chem. Phys. Lett. 383 (2004) 601.
[37] J.C. Robinson, N.E. Sveum, D.M. Neumark, J. Chem. Phys. 119 (2003) 5311.
[38] P.A. Heimann, M. Koike, C.W. Hsu, D. Blank, X.M. Yang, A.G. Suits, Y.T. Lee, M. Evans, C.Y. Ng, C. Flaim, H.A. Padmore, Rev. Sci. Instrum. 68 (1997) 1945.
[39] A.G. Suits, P.A. Heimann, X.M. Yang, M. Evans, C.W. Hsu, K.T. Lu, Y.T. Lee, A.H. Kung, Rev. Sci. Instrum. 66 (1995) 4841.
[40] A.J.C. Nicholson, J. Chem. Phys. 39 (1963) 954.
[41] F. Qi, R. Yang, B. Yang, C. Huang, L. Wei, J. Wang, L. Sheng, Y. Zhang, Rev. Sci. Instrum. 77 (2006) 084101.
[42] J.C. Person, P.P. Nicole, J. Chem. Phys. 53 (1970) 1767.
[43] P.K. Sharma, E.L. Knuth, W.S. Young, J. Chem. Phys. 64 (1976) 4345.
[44] E.L. Knuth, Engine Emissions: Pollutant Formation and Measurement, Plenum, New York, 1973.
[45] T.A. Cool, K. Nakajima, C.A. Taatjes, A. Mcllroy, P.R. Westmoreland, M.E. Law, A. Morel, Proc. Combust. Inst. 30 (2005) 1681.
[46] J.D. Bittner, Ph.D. Thesis, vol. 3, Massachusetts Institute of Technology, 1981.
[47] P.J. Linstrom, W.G. Mallard, NIST Chemistry WebBook, NIST Standard Reference Database Number 69, National Institute of Standards and Technology, Gaithersburg, MD, 2003.
[48] H. Koizumi, J. Chem. Phys. 95 (1991) 5846.
[49] C. Backx, G.R. Wight, R.R. Tol, M.J. Van Der Wiel, J. Phys. B: Mol. Phys. 8 (1975) 3007.
[50] W.A. Chupka, J. Berkowitz, J. Chem. Phys. 47 (1967) 2921.
[51] J.W. Au, G. Cooper, G.R. Burton, T.N. Olney, C.E. Brion, Chem. Phys. 173 (1993) 209.
[52] J.W. Au, G. Cooper, C.E. Brion, Chem. Phys. 173 (1993) 241.
[53] F.P. Lossing, J.C. Traeger, Int. J. Mass Spectrom. Ion Phys. 19 (1976) 9.
[54] M.J.S. Dewar, S.D. Worley, J. Chem. Phys. 50 (1969) 654.
[55] K.V. Wood, J.W. Taylor, Int. J. Mass Spectrom. Ion Phys. 30 (1979) 307.
[56] J.C. Traeger, J. Phys. Chem. 90 (1986) 4114.
[57] W.A. Brand, T. Baer, J. Am. Chem. Soc. 106 (1984) 3154.
[58] F.S. Ashmore, A.R. Burgess, J. Chem. Soc. Faraday Trans. 2 74 (1978) 734.
[59] G. Bieri, F. Burger, E. Heilbronner, J.P. Maier, Helv. Chim. Acta 60 (7) (1977) 2213.
[60] P. Osswald, U. Struckmeier, T. Kasper, K. Kohse-Höinghaus, J. Wang, T.A. Cool, N. Hansen, P.R. Westmoreland, J. Phys. Chem. A 111 (2007) 4093.
[61] D.A. Sweigart, D.W. Turner, J. Am. Chem. Soc. 94 (1972) 5592.
[62] J.C. Traeger, R.G. McLouglin, A.J.C. Nicholson, J. Am. Chem. Soc. 104 (1982) 5318.
[63] Y.J. Shi, R.H. Lipson, Can. J. Chem. 83 (2005) 1891.
[64] F.M. Benoit, A.G. Harrison, J. Am. Chem. Soc. 99 (1977) 3980.
[65] R.H. Staley, R.D. Wieting, J.L. Beauchamp, J. Am. Chem. Soc. 99 (1977) 5964.
[66] T. Nakayama, K. Watanabe, J. Chem. Phys. 40 (1964) 558, 2213.
[67] K. Kimura, S. Katsumata, A.Y.T. Yamazaki, S. Iwata, Handbook of HeI Photoelectron Spectra of Fundamental Organic Compounds, Japan Scientific Soc. Press, Tokyo, 1981.
[68] U. Weidner, A. Schweig, J. Organometal. Chem. 39 (1972) 261.
[69] P. Masclet, G. Mouvier, J. Chim. Phys. 78 (1981) 99.